An Infrared Spectroscopic Study of the Secondary Structure of Protein Kinase Cα and Its Thermal Denaturation†

Alejandro Torrecillas, Senena Corbalán-García, and Juan C. Gómez-Fernández*

Departamento de Bioquímica y Biología Molecular (A), Facultad de Veterinaria, Universidad de Murcia. Apartado de Correos 4021, E-30080-Murcia, Spain

Received June 30, 2003; Revised Manuscript Received December 15, 2003

ABSTRACT: The secondary structure of protein kinase Cα (PKCα) has been studied using infrared spectroscopy in the presence of both H_2O and D_2O buffers. In the absence of ligands at 20 °C, it was shown that β-sheet is the major component, representing about 44% of the total structure, whereas the α-helix amounts to 22%. The addition of Ca^{2+} produced only small changes in the secondary structure at 20 °C with the β-sheet increasing up to 48%. On the other hand, the other ligands, such as phorbol 12-myristate 13-acetate (PMA), ATP, and phospholipids, did not produce any significant change. When the thermal unfolding of PKCα was studied after heating to 75 °C, the presence of the ligands affected the unfolding process. PKCα was better preserved from thermal denaturation in the presence of Ca^{2+}, the aggregated β-sheet at 1618 cm^{-1} decreasing from 19% in the absence of this ligand to 13% in its presence. Protection was also afforded by the presence of PMA or phospholipids. A two-dimensional correlation study of the denaturation of PKCα in the presence of these different ligands also showed differences among them. Synchronous 2D-IR correlation showed that the main change occurred at 1616−1619 cm^{-1}, this component being assigned to the intermolecular aggregated β-sheet of the denaturated protein. This increase was mainly correlated with the change in the α-helix component in all cases except in the presence of a mixture of ligands including Ca^{2+}, ATP, PMA, and phospholipids, when the intermolecular aggregation of β-sheet was correlated with the change in the β-sheet component. In addition, the asynchronous 2D-IR correlation study of PKCα showed that the aggregated β-sheet increased after changes in other components. It was interesting that α-helix changed before the β-sheet in the control experiment and in the presence of Ca^{2+}, while the order of change was reversed when PMA was added.

Protein kinase C (PKC)[1] is a family of related protein kinases that play an important role in regulating cell growth because they are involved in several intracellular pathways that end in transcription. PKCs include at least 10 different mammalian isoforms that can be classified into three groups according to their structure and cofactor regulation. The first group includes the classical PKC isoforms (α, βI, βII, and γ) that are regulated by acidic phospholipids, diacylglycerol, and phorbol esters and also by calcium. The second group corresponds to the novel PKC isoforms (δ, ϵ, η, and θ) that are regulated by phospholipids, diacylglycerols, and phorbol esters but not by calcium. The third group comprises the atypical PKC isoforms (ζ, τ/λ, and μ) that are not regulated by diacylglycerol or by calcium (*1*−*3*). PKC isozymes participate in the processes that regulate cell signaling, which begin in cell membranes with the appearance of bioactive derivatives of phosholipids such as diacylglycerols (*4*).

Classical PKCs consist of a single polypeptide chain comprising a regulatory region in the amino end with a size of between 20 and 40 kDa and a catalytic region in the carboxyl end with an approximate size of 45 kDa (*5*−*6*). Four conserved domains can be found in classical PKCs (called C1−C4) always with five variable regions, known as V1−V5 (*6*). The functions of these domains have been characterized by biochemical studies and by site-directed mutagenesis. In this way, classical PKCs are activated by their translocation to membranes in a process regulated by two kinds of molecular signals. The first signal is calcium, which binds to the protein C2 domain that is always present in classical PKCs (*6*) before interacting with the charged groups of anionic phospholipids (*7*). The second signal is diacylglycerol, which binds to the protein C1 domain that, in classical PKCs, occupies the amino-terminal position. Phorbol esters are tumor-promoters that also bind to the C1-domains of classical PKCs (*8*). The catalytic region contains the C3 domain, which includes the ATP binding site, and the C4 domain, which includes the substrate binding site (*9*).

To date, it has not been possible to determine the high-resolution structure of any PKC, although it has been possible to obtain the structure of several domains. For example, the

† This work was supported by Grants BMC2002-00119 from Dirección General de Investigación, Ministerio de Ciencia y Tecnología (Spain), and PI-35/00789/FS/01 from Fundación Séneca (Comunidad Autónoma de Murcia, Spain). A.T. is a recipient of a fellowship from Fundación Séneca (Murcia, Spain). S.C.-G. belongs to "Ramón y Cajal Program" supported by Ministerio de Ciencia y Tecnología y Universidad de Murcia.

* Corresponding author. Telephone: +34-968-364766. Fax: +34-968-364766. E-mail: jcgomez@um.es.

[1] Abbreviations: ATP, adenosine-5′-triphosphate; LUVs, large unilamellar vesicles; PIP_2, phosphatidylinositol 4,5-bisphosphate; PKC, protein kinase C.; PMA, phorbol 12-myristate 13-acetate; POPA, 1-palmitoyl-2-oleoyl-*sn*-glycero-3-phosphate; POPC, 1-palmitoyl-2-oleoyl-*sn*-glycero-3-phosphocholine; SUVs, small unilamellar vesicles.

10.1021/bi035128i CCC: $27.50
Published on Web 02/06/2004

structure of the C1 domains from PKCδ (*10*), PKCα (*11*), and PKCγ (*12*) are characterized by cysteine-rich sequences, which form zinc-fingers, and adopt a globular structure with two antiparallel β-sheets and a small α-helix in the carboxylic end. The C1 domain binds phorbol esters without any variation in the structure (*10*). A number of works have also been published on the high-resolution structure of the C2 domain from PKCβI (*13*), PKCδ (*14*), PKCα (*7*, *15*), and PKCε (*16*). The structure of this domain consists of eight antiparallel β-sheets forming a β-sandwich. This activation of PKC involves the interaction of the domain through a Ca^{2+} bridge with the membrane by using the high-affinity binding site rich in acidic residues such as aspartic acid (*7*, *15*). The C2 domain from PKCα may also bind phosholipids in a Ca^{2+}-independent site rich in lysines (*15*), which may serve for the activation of PKCα by PIP_2 (*17*).

Although the high-resolution structure of the catalytic region is not known, a model has been proposed for PKCβII (*18*) based on the structure of protein kinase A (PKA) (*19*). The proposed structure assumes the existence of a cavity corresponding to the active site that will be blocked by the pseudosubstrate in the inactive state of the protein (*19*). A model has been proposed for the whole structure of PKCα based on previously known structures of different domains (*20*).

Very few studies have been carried out with the full-length protein because so far it has proved impossible to obtain crystals of sufficient quality to carry out high-resolution studies. Nevertheless, some low-resolution studies have been performed with microcrystals of the PKCβ, providing information on its size and shape (*21*), while other studies have used two-dimensional crystals of PKCδ and PKCα (*22*−*23*). Finally, other low-resolution studies have focused on the circular dichroism of the secondary structure of PKC (*24*, *25*), although such studies were carried out with protein preparations isolated from biological tissues and consisting of a mixture of isoenzymes.

Infrared spectroscopy is a very well suited technique to study the secondary structure of proteins (*26*). Two-dimensional infrared (2D-IR) correlation spectroscopy (*27*−*29*) is a modern technique with a very broad potential in the study of proteins. This technique has four main advantages: (1) The 2D-IR correlation spectroscopy deconvolutes amide bands into component bands due to different secondary structures. (2) It allows the establishment of correlations between bands due to different secondary structures of protein through selective correlation peaks for a given conformation. (3) It enables us to monitor intensity variations even in very weak protein bands. (4) It provides information about specific order of secondary structural changes and changes under various environments (*29*).

In the present study, we use highly purified cloned PKCα from *Sf9* insect cells to carry out a study on the secondary structure of this enzyme using infrared spectroscopy. We have also studied the thermal unfolding of this protein and the effect produced by several protein ligands, which act as activators. Finally, 2D correlation spectroscopy was used to further clarify the unfolding path of the protein during the thermal denaturation and the effect on it of the different ligands.

EXPERIMENTAL PROCEDURES

Materials. 1-Palmitoyl-2-oleoyl-*sn*-glycero-3-phosphocholine (POPC) and 1-palmitoyl-2-oleoyl-*sn*-glycero-3-phosphate (POPA) were purchased from Avanti Polar Lipids, Inc. (Alabaster, AL). Adenosine-5′-triphosphate (ATP) was purchased from Roche (Roche Diagnostics, Barcelona, Spain). Calcium standard and phorbol 12-myristate 13-acetate (PMA) were obtained from Sigma (Madrid, Spain). Western Lightning Chemiluminescence Reagent Plus was purchased from NEN (Boston, MA). Deuterated water (deuterium oxide) was purchased from Aldrich (Aldrich Chemical Co., Milwaukee, WI). Water was twice distilled and deionized using a Millipore system from Millipore Ibérica (Madrid, Spain).

Preparation of Phospholipids. Lipid vesicles were generated by mixing chloroform solutions of POPC and POPA at the desired proportions (POPC/POPA, molar ratio 1:4). Lipids were dried from the organic solvent under a stream of oxygen-free nitrogen, and then the last traces of organic solvent were removed under vacuum for at least 2 h. Dried phospholipids were resuspended in the appropriate buffer by vigorous vortexing. To produce small unillamelar vesicles (SUVs), phospholipid mixtures were subjected to direct probe sonication (10 cycles of 15 s). Large unillamelar vesicles (LUVs) were prepared as previously described (*30*). Briefly, phospholipid mixtures were frozen and thawed at 30 °C five times and then passed through two polycarbonate filters with a 0.1 μm pore size using an extruder (Lipex Biomembranes Inc., Canada).

Expression and Purification of Protein Kinase Cα. The full length cDNA for porcine PKCα was kindly provided by Dr. Robert M. Bell (Duke University Medical Center, Durham, NC). PKCα was expressed in *Sf9* (*Spodoptera frugiperda*) insect cells, and the protein was purified as described previously (*31*−*33*). Briefly, *Sf9* cells were infected with a high-titer recombinant baculovirus, and then PKCα was purified to homogeneity from the cytosolic fraction using chromatographic techniques. Finally, PKCα was concentrated using an Ultrafree-30 centrifugal filter device (Millipore Inc., Bedford, MA), and the concentration was determined using the method described by Smith el al. (*34*). The purity of the sample was checked by silver staining, and it was higher than 95%.

PKCα Membrane Binding Assay. To verify that PKCα is bound to the membranes used in the conditions of the FT-IR assays, sucrose-loaded large unillamelar vesicles (LUVs) were used. Lipid mixtures (POPC/POPA, molar ratio 1:4) and LUVs were prepared as described above. Dried phospholipids were resuspended in 25 mM Tris-HCl, pH 7.5, 100 mM NaCl, 1 mM EGTA, 250 mM sucrose, and 1 mM DTT by vigorous vortexing. The mixtures were frozen and thawed at 30 °C five times. Then they were passed through two polycarbonate filters with a 0.1 μm pore size using an extruder (Lipex Biomembranes Inc., Canada). Fifty micrograms of PKCα and 200 μg of lipid mixture were used for each sample with a final volume of 200 μL. The experiments were carried out using different free Ca^{2+} concentrations. Note that the molar ratio (protein/phospholipid) used in these experiments was the same as that used in the FT-IR assays. The binding mixture was incubated at 25 °C for 10 min before adding the protein. The binding buffer contained the same components as the buffer that was used for resuspend-

ing the lipid mixture. The binding assay ended after 20 min at 25 °C, and the vesicle-bound protein was separated from the free protein by ultracentrifugation of the mixture at 100 000 × *g* for 60 min at 15 °C. Control experiments without lipids and in the presence of vesicles but absence of calcium were carried out. Free and lipid-bound PKCα were detected by Western Blotting as previously described (*35*). The amount of protein loaded into the SDS−polyacrylamide gel was in the linear range of detection of the Chemiluminiscence Western Blotting kit.

IR Spectroscopy. PKCα was prepared at 20 mg·mL^{-1} (240 μM) in H_2O buffer and at 5 mg·mL^{-1} (60 μM) in D_2O buffer, containing in both cases 25 mM Tris-HCl, pH 7.5 (or pD 7.5), 100 mM NaCl, 0.5 mM EGTA, and 0.5 mM DTT. When D_2O buffer was used, the protein was incubated overnight at 4 °C to maximize H−D exchange. To study infrared amide bands of the protein in the presence of lipids, SUVs were prepared in the same buffer, and they were mixed with the protein solutions. The lipid mixtures used in these experiments contained POPC/POPA (molar ratio 1:4) and were prepared at 80 mg·mL^{-1} (when using H_2O buffer) or 20 mg·mL^{-1} (when using D_2O buffer). The protein−lipid mixtures were centrifuged, and only the protein present in the pellet, that is, bound to the lipid membranes, was used for FT-IR analysis.

Infrared spectra were recorded using a Bruker Vector 22 Fourier transform infrared spectrometer equipped with a MCT detector. Samples were examined in a thermostated Specac 20710 cell (Specac, Kent, U.K.) equipped with CaF_2 windows and 6 μm spacers (H_2O buffer) or 25 μm spacers (D_2O buffer). The spectra were recorded after equilibration of the samples at 20 °C for 20 min in the infrared cell. A total of 128 scans were accomplished for each spectrum with a nominal resolution of 2 cm^{-1}, and then spectra were Fourier transformed using a triangular apodization function. A sample shuttle accessory was used to obtain the average background and sample spectra. The sample chamber of the spectrometer was continuously purged with dry air to prevent atmospheric water vapor from obscuring the bands of interest. Samples were scanned between 20 and 75 °C at 5 °C intervals with a 5 min delay between each scan using a circulation water bath interfaced to the spectrometer computer. Spectral subtraction was performed interactively using the Grams/32 program (Galactic Industries Corporation, Salem, NH). Solvent contribution was eliminated by subtracting the pure buffer spectrum from the protein sample one to maintain a flat baseline between 2000 and 1300 cm^{-1}, as previously described (*36*). This procedure eliminated the possible water contamination because the water band at 2150 cm^{-1} was abolished when using D_2O buffers (*37*). Finally, the spectra were subjected to a baseline in the amide I or I′ regions (1700−1600 cm^{-1}) to improve the curve fitting and then to second-derivation and deconvolution, according to Griffiths and Pariente (*38*), using the Grams/32 software. Fourier self-deconvolution was carried out using a Bessel smoothing function, a Lorentzian shape with a γ factor of 10, and a full width at half-height of 20 cm^{-1}. Both deconvolution and derivation gave the number and position, as well as an estimation of the bandwidth and the intensity of the bands, making up the amide I region. Thereafter, curve fitting was performed and the heights, widths, and positions of each band were optimized successively. Data treatment and band decomposition of the original amide I or amide I′ regions have been previously described (*36*, *39*, *40*). The fractional areas of the bands in the amide I or amide I′ regions were calculated from the final fitted band areas. It is assumed that the extinction coefficients of the different protein components are not very different among them and that, in any case, the error derived from this assumption is within the range of errors inherent to the method (see the Discussion section).

The signal-to-noise ratio was calculated through the ratio of intensities between the maximum of the amide I band at 1636 cm^{-1} and the intensity at a frequency out of this region and where no significant absorbance takes place such as 1780 cm^{-1}, and this was found to be about 600 in all the samples studied.

The procedure used here to quantitatively calculate the secondary structure is usually assumed to have an error of about 1% (*39*), and in this paper, we have assumed it to be 1−2% as deduced from the comparison of at least three independent experiments and the repetition of the fitting procedure by three different persons; therefore, we will assume as being significantly different changes in the structural components higher than 3%.

Two-dimensional correlation analysis was carried out using the 2D-Pocha program written by Dr. Adachi and Dr. Y. Ozaki (Kwansei Gakuin University, Japan), which can be found at the following website: http://science.kwansei.ac.jp/~ozaki/2D-Pocha.htm. This software can calculate the two-dimensional correlation spectroscopy proposed by I. Noda (*27*). The maximum intensity of the whole correlation map is divided by 6 giving place to a contour map in which the main peak, that is, the one with the maximum intensity, will be surrounded by six contour lines and the rest of the peaks will show a number of contour lines that will reflect their intensities in relation to the main peak.

To obtain the 2D-IR maps, heating was used as the perturbation to induce time-dependent spectral fluctuations and to detect dynamical spectral variations on the secondary structure of the PKCα. The mathematical background for generalized 2D correlation spectroscopy has been described in detail (*27*). The following procedures were taken to obtain generalized 2D correlation of temperature-dependent infrared spectra. Given an infrared spectral intensity variation $A(\nu,T)$ observed in a temperature range between T_{min} and T_{max}, the synchronous and asynchronous 2D-IR correlation intensities, $\Phi(\nu_1,\nu_2)$ and $\Psi(\nu_1,\nu_2)$, become

$$\Phi(\nu_1,\nu_2) + i\Psi(\nu_1,\nu_2) = \frac{1}{\pi(T_{max} - T_{min})}\int_0^\infty Y_1(\omega)Y_2^*(\omega)\,d\omega$$

where $Y_1(\omega)$ is the temperature-domain Fourier transform of $A(\nu_1,\nu_2)$ and $Y_2^*(\omega)$ is the conjugate of the Fourier transform of $A(\nu_2,T)$.

As reviewed by Noda (*27*), the synchronous 2D correlation spectrum of dynamic spectral intensity variations represents the simultaneous coincidental changes of spectral intensities measured at ν_1 and ν_2. Correlation peaks appear at both diagonal (autopeaks) and off-diagonal peaks (cross-peaks). The asynchronous spectrum of dynamic spectral intensity variations represents sequential, or unsynchronized, changes of spectral intensities measured at ν_1 and ν_2. The asynchro-

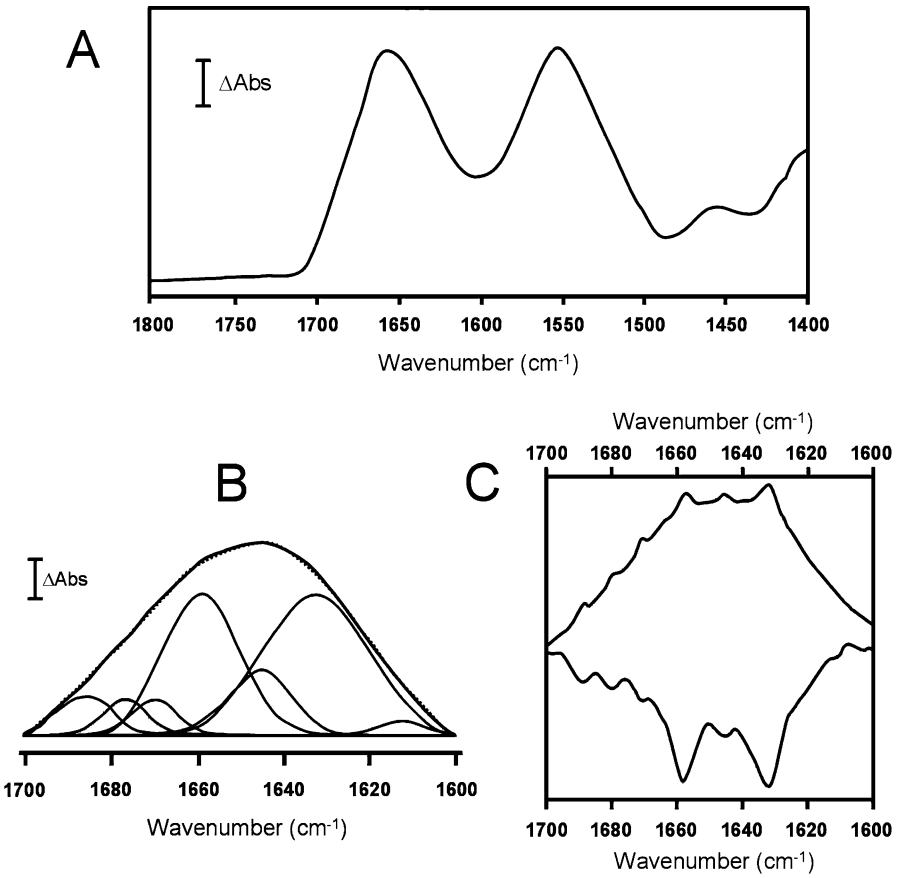

FIGURE 1: FT-IR spectra of PKCα in H_2O buffer in the presence of 200 μM EGTA at 20 °C. The protein concentration was 20 mg·mL^{-1} (240 μM). The increment in absorbance units (ΔAbs) was 0.04. Panel A shows the FT-IR difference spectrum in the range between 1800 and 1400 cm^{-1}, where the amide I and amide II regions can be seen. Panel B shows the FT-IR spectrum (solid line) in the amide I region with the fitted component bands. The parameters corresponding to the component bands are shown in Table 1. The dashed line represents the curve-fitted spectrum. Panel C shows the deconvolution (upper trace) and second derivative (lower trace) of the FT-IR spectrum of this sample.

Table 1: FT-IR Parameters of the Amide I Band Components of PKCα (20 mg·mL^{-1}) in H_2O Buffer at 20 °C and in the Presence of 200 μM EGTA (A), 2.4 mM Ca^{2+} (B), 2 mM PMA with 4 μM $ZnCl_2$ (C), 2 mM ATP with 4 μM $ZnCl_2$ (D), and 1 mM Ca^{2+}, 2 mM ATP, 2 mM PMA, and 112.8 mM (80 mg·mL^{-1}) POPC/POPA (1:4 Molar Ratio) in the Presence of 4 μM $ZnCl_2$ (E)

	A		B		C		D		E	
assignment	position[a] (cm^{-1})	area[b] (%)	position (cm^{-1})	area (%)	position (cm^{-1})	area (%)	position (cm^{-1})	area (%)	position (cm^{-1})	area (%)
antiparallel β-sheet	1688	7	1689	7	1688	8	1688	8	1689	6
β-turns	1678	5	1678	5	1678	6	1678	6	1678	7
β-turns	1670	5	1671	5	1671	6	1670	7	1670	7
α-helix + random	1658	29	1658	28	1658	28	1658	28	1657	28
open loops	1644	12	1644	10	1645	12	1645	12	1644	12
β-sheet	1631	42	1631	45	1632	40	1632	40	1631	40

[a] Peak position of the amide I band components. [b] Percentage area of the amide I band components. The area corresponding to side chain contributions located at 1600−1615 cm^{-1} has not been considered.

nous spectrum has no autopeaks, consisting exclusively of cross-peaks located at off-diagonal positions. An asynchronous cross-peak develops only if the intensities of two dynamic spectral intensities vary out of phase with each other for some Fourier-frequency components of signal fluctuations.

RESULTS

FT-IR Studies. The secondary structure of PKCα was studied using infrared spectroscopy. Spectra were obtained using both H_2O buffer and D_2O buffer. Figure 1A shows the spectrum obtained in H_2O buffer of the native PKCα (20 mg·mL^{-1}) in the presence of 200 μM EGTA, that is, in the absence of ligands, at 20 °C.

The amide I band decomposition of the native PKCα in H_2O and 200 μM EGTA at 20 °C is shown in Figure 1B. The number and initial position of the component bands were obtained from band-narrowed spectra by Fourier deconvolution and derivation (Figure 1C). The corresponding parameters, that is, band position, percentage area, bandwidth of each spectral component, and assignment, are shown in Table 1. The spectrum in H_2O showed six components in the amide I region. The main component accounting for 42% of the total band area was localized at 1631 cm^{-1}, and it

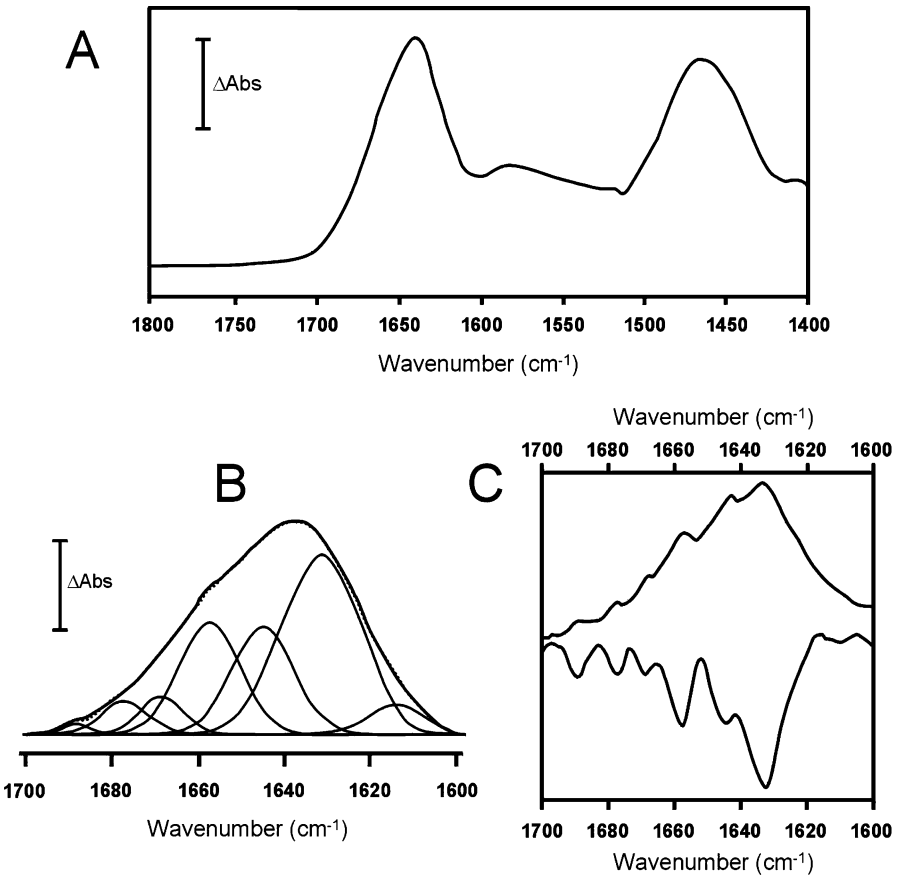

FIGURE 2: FT-IR spectra of PKCα in D_2O buffer in the presence of 200 μM EGTA at 20 °C. The protein concentration was 5 mg·mL^{-1} (60 μM). The increment in absorbance units (ΔAbs) was 0.04. Panel A shows the FT-IR difference spectrum in the range between 1800 and 1400 cm^{-1}, where the amide I′, amide II, and amide II′ regions can be seen. Panel B shows the FT-IR spectrum (solid line) in the amide I′ region with the fitted component bands. The parameters corresponding to the component bands are shown in Table 2. The dashed line represents the curve-fitted spectrum. Panel C shows the deconvolution (upper trace) and second derivative (lower trace) of the FT-IR spectrum of this sample.

can be assigned to β-structure (*26*). The component localized at 1658 cm^{-1} that contributes 29% of the total area may be assigned to either α-helix or disordered structure (*26*). The components appearing at 1678 cm^{-1} (5%) and 1670 cm^{-1} (5%) arise from β-turns (*41*, *42*), and the component centered at 1688 cm^{-1} (7%) was assigned to antiparallel β-sheet (*26*). Another component was located at 1644 cm^{-1}, and it is assigned to open loops, that is, to loops fully hydrated and not interacting with nearby amide functional groups (*43*−*45*). In summary, the secondary structure of PKCα in H_2O buffer in the presence of EGTA was 49% β-pleated sheet, after adding the areas of components at 1631 and 1688 cm^{-1}, 29% assigned to α-helix and disordered structures, 12% to open loops, and 10% β-turns (Table 1).

Very similar results (Table 1) were obtained for the secondary structure of this protein, differences of only 1−3% being obtained in some components, which is within experimental error, when the spectrum was taken in the presence of several ligands, such as 2.4 mM Ca^{2+}, with a protein/Ca^{2+} molar ratio of 1:10. Among other ligands that did not induce changes higher than 3% at 20 °C were 2 mM PMA with 4 μM $ZnCl_2$, 2 mM ATP with 4 μM $ZnCl_2$, and a mixture of ligands including Ca^{2+} (1 mM), ATP (2 mM), PMA (2 mM), and 80 mg·mL^{-1} (112.8 mM) POPC/POPA (1:4 molar ratio) in the presence of 4 μM $ZnCl_2$ (Table 1).

In a second set of experiments, spectra were obtained in the presence of D_2O buffer for a sample of the native PKCα (5 mg·mL^{-1}) in the presence of 200 μM EGTA at 20 °C (Figure 2A). It can be observed that the amide II band, which was observed in samples prepared in the presence of H_2O buffer and centered at about 1560 cm^{-1}, has decreased very considerably as a consequence of the use of D_2O buffer. This is the consequence of the H−D exchange that takes place when using D_2O buffer. The range of H−D exchange was quantified using two different procedures. The first one implies the calculation of the ratio between the areas of amide II and amide I bands (*46*). If we suppose that the value obtained for the sample in H_2O buffer is 100%, the value obtained for this sample in the presence of D_2O buffer was 13.3%, and hence, the exchange was 86.7%. Similar values were obtained for all the other samples studied in this paper ranging between 83.8% and 87.1%. These percentages seem to be related to maximum exchange, since after heating at 75 °C, that is, denaturation, the percentage of exchange increased but very slightly, ranging between 83.0% and 85.5%. The second procedure consisted in obtaining the ratio between the values of absorbances at 1550 (amide II) and that of the band at 1515 cm^{-1}, which corresponds to tyrosine. This last band at 1515 cm^{-1} is used to normalize data since it is not affected by the H−D exchange (*47*). Ratio values obtained from the samples studied in D_2O buffer can then be compared with those obtained in the presence of H_2O buffer. The results were very similar to those found through the first procedure with percentages of exchange ranging

Table 2: FT-IR Parameters of the Amide I′ Band Components of PKCα (5 mg·mL^{-1}) in D_2O Buffer at 20 °C and in the Presence of 200 μM EGTA (A), 600 μM Ca^{2+} (B), 500 μM PMA with 1 μM $ZnCl_2$ (C), 500 μM ATP with 1 μM $ZnCl_2$ (D), and 250 μM Ca^{2+}, 500 μM ATP, 500 μM PMA, and 28.2 mM (20 mg·mL^{-1}) POPC/POPA (1:4 Molar Ratio) in the Presence of 1 μM $ZnCl_2$ (E)

	A		B		C		D		E	
assignment	position[a] (cm^{-1})	area[b] (%)	position (cm^{-1})	area (%)	position (cm^{-1})	area (%)	position (cm^{-1})	area (%)	position (cm^{-1})	area (%)
β-turns	1690	1	1690	1	1685	2	1686	2	1689	1
antiparallel β-sheet	1676	5	1677	4	1674	7	1674	8	1677	4
β-turns	1659	6	1659	5	1664	7	1663	12	1666	9
α-helix	1657	22	1657	20	1655	22	1652	19	1655	21
random + open loops	1644	22	1644	22	1643	20	1642	19	1644	21
β-sheet	1631	44	1631	48	1631	42	1630	40	1631	44

[a] Peak position of the amide I′ band components. [b] Percentage area of the amide I′ band components. The area corresponding to side chain contributions located at 1600−1615 cm^{-1} has not been considered.

between 82.8% and 85.5% at 20 °C and 84.6% and 85.3% at 75 °C for all the samples studied, hence confirming that the heating to 75 °C did not appreciably enhanced the H−D exchange.

The amide I′ band decomposition of the native PKCα in D_2O and 200 μM EGTA at 20 °C is shown in Figure 2B. The number and initial position of the component bands were obtained from band-narrowed spectra by Fourier deconvolution and derivation (Figure 2C). The corresponding parameters, that is, band position, percentage area, bandwidth of each spectral component, and assignment, are shown in Table 2. The spectra in D_2O exhibit six component bands in the 1700−1600 cm^{-1} region, and the quantitative contribution of each band to the total amide I′ contour was obtained by band curve-fitting of the original spectra. The major component in the amide I′ region appears at 1631 cm^{-1} and clearly arises from intramolecular C═O vibrations of the β-sheets (*26*, *36*, *39*), this being at the same frequency as that in H_2O (see Table 1 above). The high-frequency component at 1676 cm^{-1} can be assigned to the antiparallel β-sheet structure (*36*, *48*), appearing at 1688 cm^{-1} in H_2O buffer. The 1657 cm^{-1} component corresponds to α-helix (*26*, *39*, *43*, *48*), and it is separated from the random component appearing in this D_2O buffer at 1644 cm^{-1}, although the band at 1644 cm^{-1} can be attributed to nonstructured conformations, including open loops (*42*, *43*) that were already observed at this frequency in the H_2O buffer. The bands located at 1669 and 1690 cm^{-1} arise from β-turns (*36*, *49*, *50*). Additionally, there is a band at about 1610 cm^{-1}, which has been assigned to side chain absorption (*39*, *50*−*52*) and of which the contribution therefore is not included in the calculation of the secondary structure of PKCα.

The secondary structure of PKCα in the presence of 200 μM EGTA in D_2O buffer was as follows: 49% β-sheet (taking into account the 1631 and 1676 cm^{-1} bands), 22% α-helix, 7% β-turns (adding the 1669 and 1690 cm^{-1} components), and 22% open loops and nonstructured conformation (see Table 2). Very similar results were obtained for the secondary structure of this protein when the spectrum was taken in the presence of several ligands, such as 600 μM Ca^{2+} with a protein/Ca^{2+} molar ratio of 1:10, differences of only 1−2% being obtained in some components, which is within experimental error. The most significant effect was the increasing of the β-sheet, which amounted 48% in these conditions. Other ligands that did not induce changes higher than 3% at 20 °C were 500 μM PMA with 1 μM $ZnCl_2$ and a mixture of ligands including Ca^{2+} (250 μM), ATP (500 μM), PMA (500 μM), and 20 mg·mL^{-1} (28.2 mM) POPC/POPA (1:4 molar ratio) in the presence of 1 μM $ZnCl_2$ (Table 2). In the case of 500 μM ATP, there were two higher differences, an increase in the β-turns component (1663 cm^{-1}), which reached 12% (6% in the absence of ligands), and a decrease in the β-sheet component (1630 cm^{-1}), which amounted to 40% (44% in the absence of the ligands) (Table 2).

To gain further insight into the structural changes that occur during ligand binding, thermal stability studies were performed. The FT-IR spectrum of PKCα in D_2O/EGTA buffer revealed major changes in the amide I′ mode at 75 °C (Figure 3A). These changes included a broadening of the overall amide I′ contour and the appearance of a well-defined component at 1618 cm^{-1}, which is highly characteristic of thermally denatured proteins, together with another new component, which is also characteristic of aggregated β-sheet, at 1679 cm^{-1} (*36*, *53*). These components indicate that extended structures were formed by aggregation of the unfolded proteins produced as a consequence of irreversible thermal denaturation (*37*, *51*, *53*, *54*). These components amounted to 19% and 8%, respectively (Table 3). Also of interest is the fact that, apart from the appearance of the 1618 cm^{-1} component, other changes in the structure resulted from protein denaturation. The spectrum corresponding to PKCα in the presence of 200 μM EGTA at 75 °C (Figure 3A) shows a band centered at 1643 cm^{-1} as the major component, which corresponds to an unordered structure and represents 33% of the total area (Table 3). The band at 1629 cm^{-1} corresponds to a β-sheet structure and shows two main changes: the percentage of the total area has decreased to 20%, and the maximum wavelength of this component has shifted from 1631 cm^{-1} at 20 °C to 1629 cm^{-1} at 75 °C (Tables 2 and 3). In addition, the α-helix component decreased from 22% to 12% at 20 °C. Thus, thermal denaturation of PKCα is characterized by irreversible aggregation and unfolding of the β-sheet structure into a disordered structure with a considerable decrease of α-helix and an increase in random structure.

The addition of 600 μM Ca^{2+}, which produced a protein/Ca^{2+} molar ratio of 1:10, afforded a certain protection so that the β-structure decreased to only 33% at 75 °C and the 1618 cm^{-1} component only amounted to 13%, while the random component only increased to 27%. The α-helix decreased to 12%, a similar percentage to that observed for

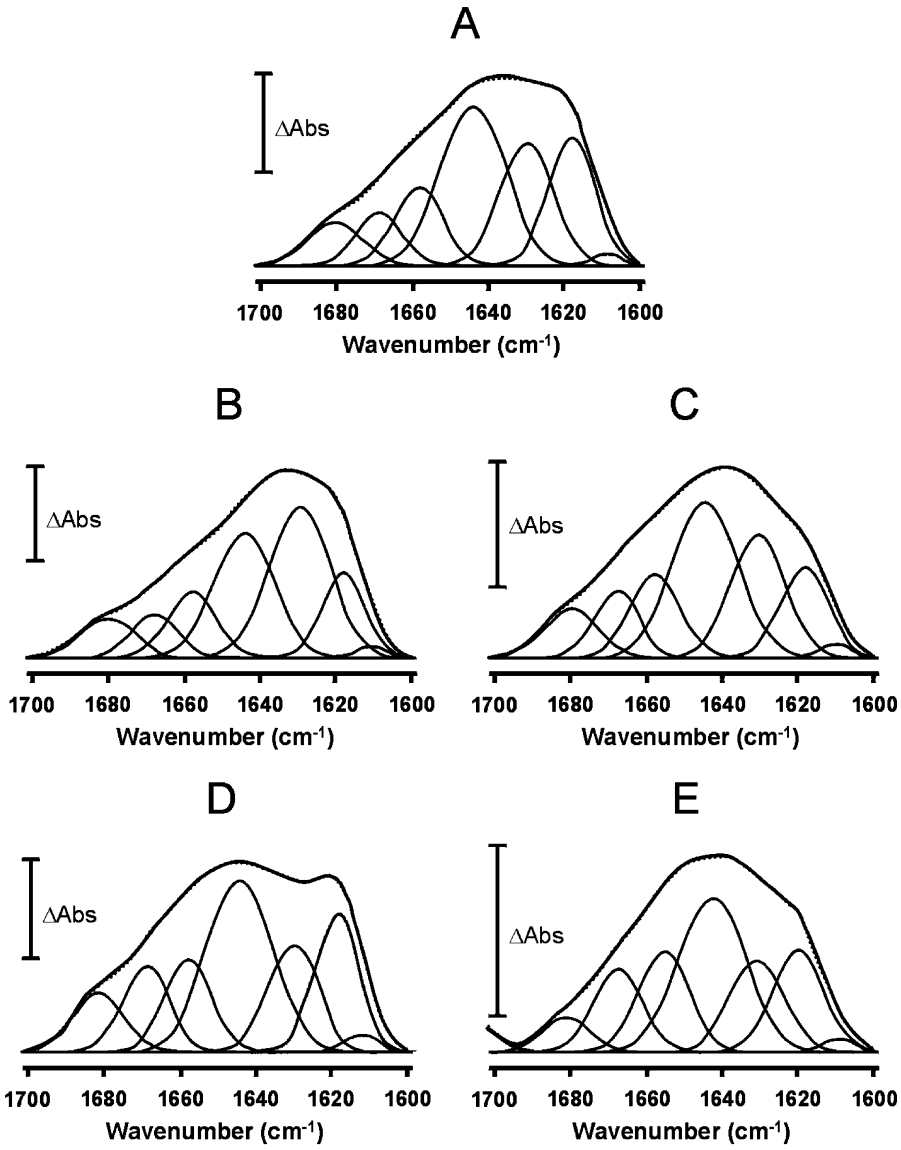

FIGURE 3: FT-IR spectra (solid line) of PKCα in D_2O buffer with the fitted component bands in the amide I′ region at 75 °C and in the presence of 200 μM EGTA (A), 600 μM Ca^{2+} (B), 500 μM PMA with 1 μM $ZnCl_2$ (C), 500 μM ATP with 1 μM $ZnCl_2$ (D), and 250 μM Ca^{2+}, 500 μM ATP, 500 μM PMA, and 28.2 mM (20 mg·mL^{-1}) POPC/POPA (1:4 molar ratio) in the presence of 1 μM $ZnCl_2$ (E). The parameters corresponding to the component bands are shown in Table 2. The dashed line represents the curve-fitted spectrum. The protein concentration was 5 mg·mL^{-1} (60 μM). The increment in absorbance units (ΔAbs) was 0.04.

Table 3: FT-IR Parameters of the Amide I′ Band Components of PKCα (5 mg·mL^{-1}) in D_2O Buffer at 75 °C and in the Presence of 200 μM EGTA (A), 600 μM Ca^{2+} (B), 500 μM PMA with 1 μM $ZnCl_2$ (C), 500 μM ATP with 1 μM $ZnCl_2$ (D), and 250 μM Ca^{2+}, 500 μM ATP, 500 μM PMA, and 28.2 mM (20 mg·mL^{-1}) POPC/POPA (1:4 Molar Ratio) in the Presence of 1 μM $ZnCl_2$ (E)

	A		B		C		D		E	
assignment	position[a] (cm^{-1})	area[b] (%)	position (cm^{-1})	area (%)	position (cm^{-1})	area (%)	position (cm^{-1})	area (%)	position (cm^{-1})	area (%)
antiparallel β-sheet	1679	8	1679	8	1679	8	1681	9	1680	5
β-turns	1667	8	1667	7	1667	10	1667	11	1667	13
α-helix	1657	12	1657	12	1657	12	1657	12	1654	16
random + open loops	1643	33	1644	27	1644	32	1644	33	1642	33
β-sheet	1629	20	1629	33	1631	23	1630	16	1630	17
aggregated β-sheet	1618	19	1618	13	1618	15	1618	19	1619	16

[a] Peak position of the amide I′ band components. [b] Percentage area of the amide I′ band components. The area corresponding to side chain contributions located at 1600−1615 cm^{-1} has not been considered.

the protein in the presence of EGTA (Table 3 and Figure 3B).

The presence of 500 μM PMA plus 1 μM $ZnCl_2$ also afforded some protection although less than was provided by Ca^{2+}. In this case, the 1618 cm^{-1} component only amounted to 15% at 75 °C, compared with 19% in the presence of EGTA, while the β-sheet structure located at 1631 cm^{-1} remained at 23% (Table 3 and Figure 3C).

Another ligand tested was 500 μM ATP in the presence of 1 μM $ZnCl_2$. This ligand also introduced some changes

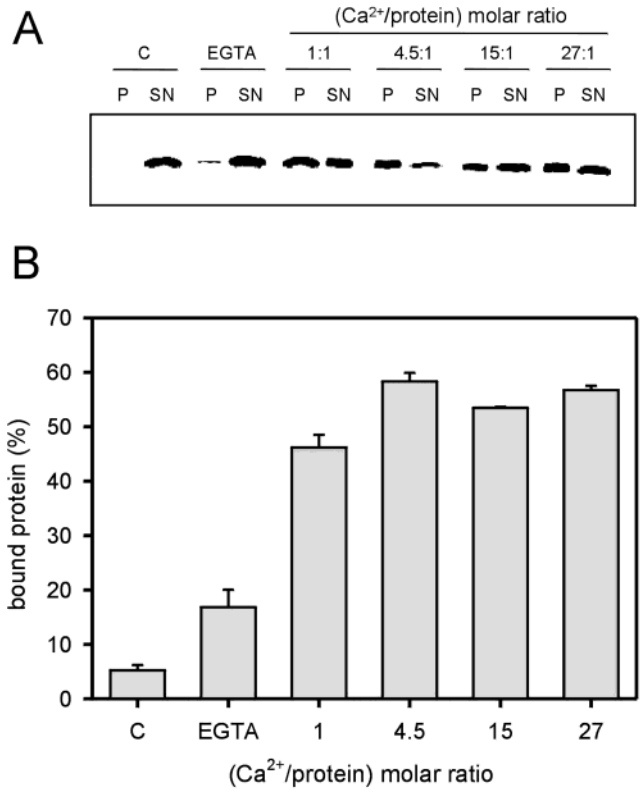

FIGURE 4: PKCα binding to membranes containing POPC/POPA (1:4 molar ratio). Fifty micrograms of PKCα and 200 μg of POPC/POPA LUVs were used to reproduce the conditions used in the FT-IR. Different Ca^{2+} concentrations were tested. The protein was detected by Western Blotting (A). The quantification of the protein (free or bound to the vesicles) was carried out by densitometry and plotted in a bar chart (B). Control assays were carried out with the protein alone in the absence of ligands (sample called C) and in the presence of LUVs without any other ligand (sample called EGTA).

in the denaturation pattern of the protein, inducing a bigger decrease in the β-structure component at 75 °C, which fell to 16%, but an increase in the percentage of β-turns, which now amounted to 11% (Table 3 and Figure 3D).

Finally, a combination of ligands including 250 μM Ca^{2+}, 500 μM ATP, 500 μM PMA, and 20 mg·mL^{-1} (28.2 mM) POPC/POPA (1:4 molar ratio) in the presence of 1 μM $ZnCl_2$ also altered the denaturation pattern with a decrease being observed in the components marking β-aggregation. These were 5% for the 1680 cm^{-1} component and 16% for the 1619 cm^{-1} component, being therefore only 21% in total (28% in the presence of EGTA). More interesting was the preservation of the α-helix component (1654 cm^{-1}) at 16% and the increase in β-turns (1667 cm^{-1}), which amounted to 13% (Table 3 and Figure 3E).

It is interesting to underline that PKCα was bound to the mixture of ligands containing Ca^{2+}, ATP, PMA, and POPC/POPA (1:4 molar ratio) in the conditions used for the FT-IR experiments, as can be seen from the binding assay depicted in Figure 4, where LUVs were used. The molar ratio (protein/phospholipid) was the same as that used in the FT-IR experiments. Free and lipid-bound PKCα were detected by Western blotting (Figure 4A), as previously described (*35*), while the quantification was carried out by densitometry (Figure 4B). Different Ca^{2+} concentrations were tested, and even in the presence of the smallest amount of

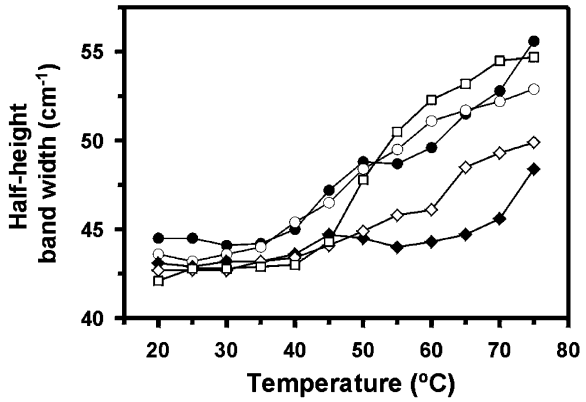

FIGURE 5: Half-height bandwidth of the amide I′ region of the FT-IR spectra in cm^{-1} as a function of temperature from 20 to 75 °C for the PKCα in D_2O buffer and in the presence of 200 μM EGTA (●), 600 μM Ca^{2+} (◆), 500 μM PMA with 1 μM $ZnCl_2$ (◇), 500 μM ATP with 1 μM $ZnCl_2$ (□), and 250 μM Ca^{2+}, 500 μM ATP, 500 μM PMA, and 28.2 mM (20 mg·mL^{-1}) POPC/POPA (1:4 molar ratio) with 1 μM $ZnCl_2$ (○).

Ca^{2+}, the protein was bound to vesicles in approximately the same proportion, that is, between 45% and 60% (Figure 4B). Control assays were carried out in the absence of ligands and in the presence of LUVs without any other ligand. It should be kept in mind that, as explained in the Experimental Procedures section, samples incubated with liposomes were centrifuged to isolate these vesicles plus bound protein and that only bound protein was present in the samples studied by infrared spectroscopy.

Figure 5 shows a plot of the half-height width of the amide I′ band against temperature, which is a way of following protein denaturation (*39*). As can be seen, the effect of the different ligands is not entirely the same: whereas Ca^{2+} (with a protein/Ca^{2+} molar ratio of 1:10) and also PMA (500 μM in the presence of 1 μM $ZnCl_2$) clearly preserve the protein from thermal-induced widening of the band, other ligands, such as ATP (500 μM with 1 μM $ZnCl_2$) and the combination of Ca^{2+} (250 μM), ATP (500 μM), PMA (500 μM), and POPC/POPA (28.2 mM) at a 1:4 molar ratio in the presence of 1 μM $ZnCl_2$, had no such effect, although, as explained, they somehow modify the denaturation pattern.

To better visualize the changes taking place during thermal denaturation, 3D-spectra were constructed (see Figure 6). A comparison was made between PKCα in the presence of 200 μM EGTA (Figure 6A) and in the presence of 600 μM Ca^{2+} (Figure 6B) or 500 μM PMA with 1 μM $ZnCl_2$ (Figure 6C). It can be clearly observed that both the widening of the overall amide I′ contour and the aggregation-indicative band at 1618 cm^{-1} were reduced in the presence of these protein ligands (Ca^{2+} and PMA).

2D-IR Correlation Studies. A deeper insight into the mechanism of protein unfolding and the role of the different ligands was obtained by 2D-IR correlation spectroscopy. In all cases, the average spectra of the temperature scans from 20 to 75 °C were used as reference in the analysis.

The synchronous 2D-IR correlation contour map of PKCα in the presence of EGTA corresponding to the heating from 20 to 75 °C (Figure 7A) shows two autopeaks located at 1617 and 1650 cm^{-1}, indicating that these are the frequencies at which the main changes are taking place during the thermally induced unfolding of the protein. The most intense

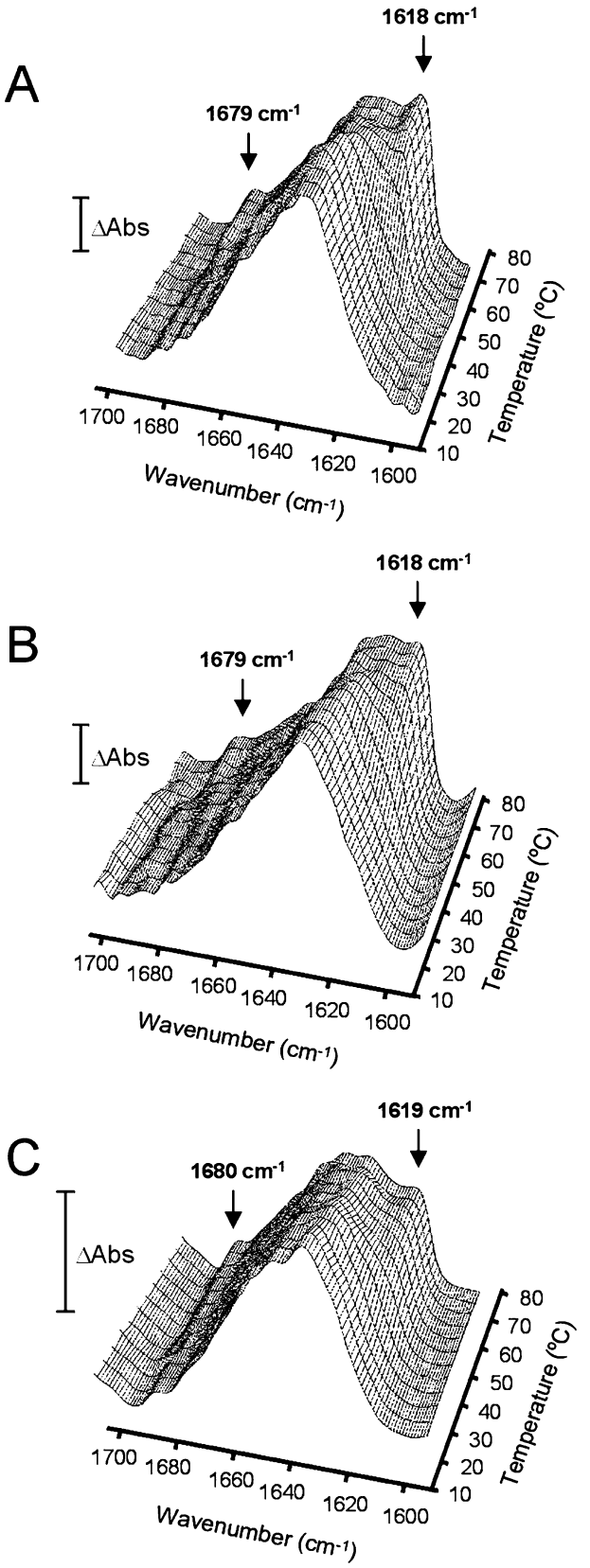

FIGURE 6: Deconvolved FT-IR spectra of PKCα in the amide I′ region (1700−1600 cm^{-1}) as a function of temperature from 20 to 75 °C in the presence of 200 μM EGTA (A), 600 μM Ca^{2+} (B), and 250 μM Ca^{2+}, 500 μM ATP, 500 μM PMA, and 28.2 mM (20 mg·mL^{-1}) POPC/POPA (1:4 molar ratio) in the presence of 1 μM $ZnCl_2$ (C). The protein concentration was 5 mg·mL^{-1} (60 μM). The bands indicating aggregation (1618−1619 cm^{-1} and 1679−1680 cm^{-1}) are shown. The increment of absorbance units (ΔAbs) was 0.04.

cross-peaks were observed at these frequencies (1617−1650 cm^{-1}) and were negative, indicating that during the heating process one of them increases as the other one decreases. These observations are fully consistent with the FT-IR studies described above: the disappearance of the α-helix component is associated with the appearance of the intermolecular aggregated β-sheet.

The presence of 600 μM Ca^{2+}, which produced a protein/Ca^{2+} molar ratio of 1:10 (Figure 7B), 500 μM PMA with 1 μM $ZnCl_2$ (Figure 7C), or 500 μM ATP with 1 μM $ZnCl_2$ (data not shown) did not modify much the synchronous spectrum, and the same peaks were observed.

The addition of the ligand combination of 250 μM Ca^{2+}, 500 μM ATP, 500 μM PMA, and 28.2 mM POPC/POPA (molar ratio 1:4) in the presence of 1 μM $ZnCl_2$ led to a change in the synchronous spectrum (Figure 7D). The autopeaks now showed their maxima at 1616 and 1635 cm^{-1}, indicating that the main correlations were now between the aggregated β-sheet and the β-sheet, respectively. The main cross-peak observed in these conditions and correlating 1616−1636 cm^{-1} was negative, meaning that the disappearance of the β-sheet was associated with the appearance of the aggregated components at 1616 cm^{-1}. Again these observations are fully consistent with the FT-IR studies described before.

The asynchronous 2D-IR correlation contour map of PKCα in the presence of EGTA due to the thermal denaturation from 20 to 75 °C (Figure 8A) showed a butterfly pattern characteristic of a bandshift (*55*) occurring toward 1617 cm^{-1} as a consequence of the aggregation accompanying denaturation. There is a maximum in this area with a negative correlation at 1617−1629 cm^{-1}, indicating that the change at 1629 cm^{-1} (decrease in β-sheet) precedes that at 1617 cm^{-1} (appearance of aggregated β-sheet). The tail of this negative peak correlates the β-sheet (1634 cm^{-1}) with the random (1649 cm^{-1}) and α-helix (1658 cm^{-1}) components, indicating that the changes at 1634 cm^{-1} (β-sheet) occurred after the other two (random and α-helix).

The asynchronous spectrum of PKCα in the presence of 600 μM Ca^{2+}, which means a protein/Ca^{2+} molar ratio of 1:10, showed a different pattern (Figure 8B) with only one significant positive peak correlating 1617−1651 cm^{-1}. Since the corresponding area in the synchronous spectrum was negative, the change in the α-helix located at 1651 cm^{-1} occurred before the aggregated β-sheet appeared (change at 1617 cm^{-1}). This positive peak was similar to another one observed in the spectrum obtained in the presence of EGTA, although the butterfly pattern corresponding to bandshift was not observed in this case, as was to be expected given the protective role of Ca^{2+}.

In the presence of 500 μM PMA with 1 μM $ZnCl_2$ (Figure 8C), a significant change was observed with respect to the control sample (in the presence of EGTA), so although a butterfly pattern was also observed, now it was positive rather than negative. However, the significance of this correlation was still the same. The maximum correlated the aggregated β-sheet with the β-sheet (1617−1636 cm^{-1}), although the corresponding area in the synchronous spectrum (Figure 7C) was now negative, so the decrease in the β-sheet (change at 1636 cm^{-1}) occurred before its aggregation (change at 1617 cm^{-1}). The resulting order of these changes was the same as that in the control sample (in the presence of EGTA). It

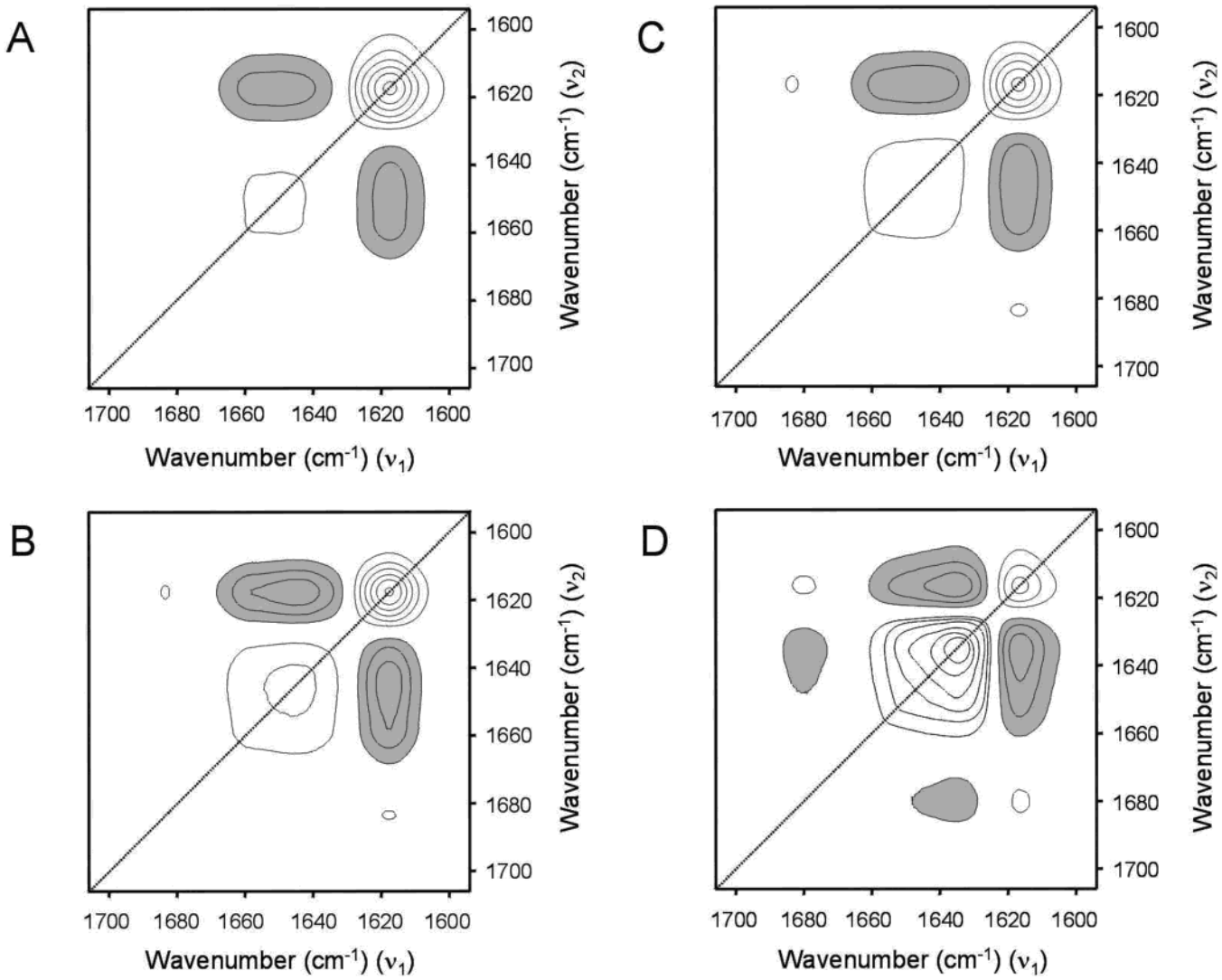

FIGURE 7: Synchronous 2D-IR correlation spectra of the PKCα in D_2O buffer as a function of temperature variation between 20 and 75 °C in the presence of 200 μM EGTA (A), 600 μM Ca^{2+} (B), 500 μM PMA with 1 μM $ZnCl_2$ (C), and the combination of 250 μM Ca^{2+}, 500 μM ATP, 500 μM PMA, and 28.2 mM (20 mg·mL^{-1}) POPC/POPA (1:4 molar ratio) in the presence of 1 μM $ZnCl_2$ (D). The correlation spectra were obtained using the 2D-Pocha program. White and dark peaks are positive and negative correlations, respectively.

seems that the autopeak appearing at 1617 cm^{-1} in the synchronous spectrum of the EGTA sample (Figure 7A) was larger and covered a larger area and hence affected the correlation located at 1617−1629 cm^{-1} in the asynchronous contour map of the control sample (Figure 8A). However, the asynchronous contour map obtained in the presence of PMA (Figure 8C) showed that there was a significant difference in the order of other changes, as can be deduced from the correlation cross-peak located at 1636−1658 cm^{-1}. Since this peak is positive, the β-sheet (1636 cm^{-1}) must change before the α-helix (1658 cm^{-1}), just the opposite of what happened with the EGTA sample.

Also the asynchronous contour map in the presence of 500 μM ATP with 1 μM $ZnCl_2$ was very similar to that of the control sample in the presence of EGTA (data not shown).

The asynchronous contour map obtained in the presence of the combination of 250 μM Ca^{2+}, 500 μM ATP, 500 μM PMA, and 28.2 mM PC/PA (molar ratio 1:4) with 1 μM $ZnCl_2$ was very similar to that obtained in the presence of EGTA (Figure 8D). The only differences detected were in the region near 1700 cm^{-1} due to the presence of phospholipid, which absorbs over this frequency.

DISCUSSION

We have studied in this work the secondary structure of PKCα, its denaturation properties, and the effect of some important ligands on the structure and denaturation properties. It should be emphasized that there is a very good agreement between the results obtained from the experiments carried out at 20 °C in the presence of H_2O (Table 1) and those in the presence of D_2O (Table 2), so the differences in percentages of β-turns and β-sheet components were always not higher than 4% in all the samples studied. Differences not higher than 4% were also detected when comparing the percentages obtained by adding the components appearing in H_2O buffer at 1658 cm^{-1} (α-helix plus random) and 1644 cm^{-1} (open loops) and on the other hand those obtained in D_2O buffer at 1657 cm^{-1} (α-helix) and at 1644 cm^{-1} (random plus open loops). This confirms the assignment of the 1644 cm^{-1} component to open loops in both H_2O and D_2O, although in the last case it also includes unordered structures. The same assignment of this component to the large loops connecting the β-strands has been made previously by other authors (*43*−*45*).

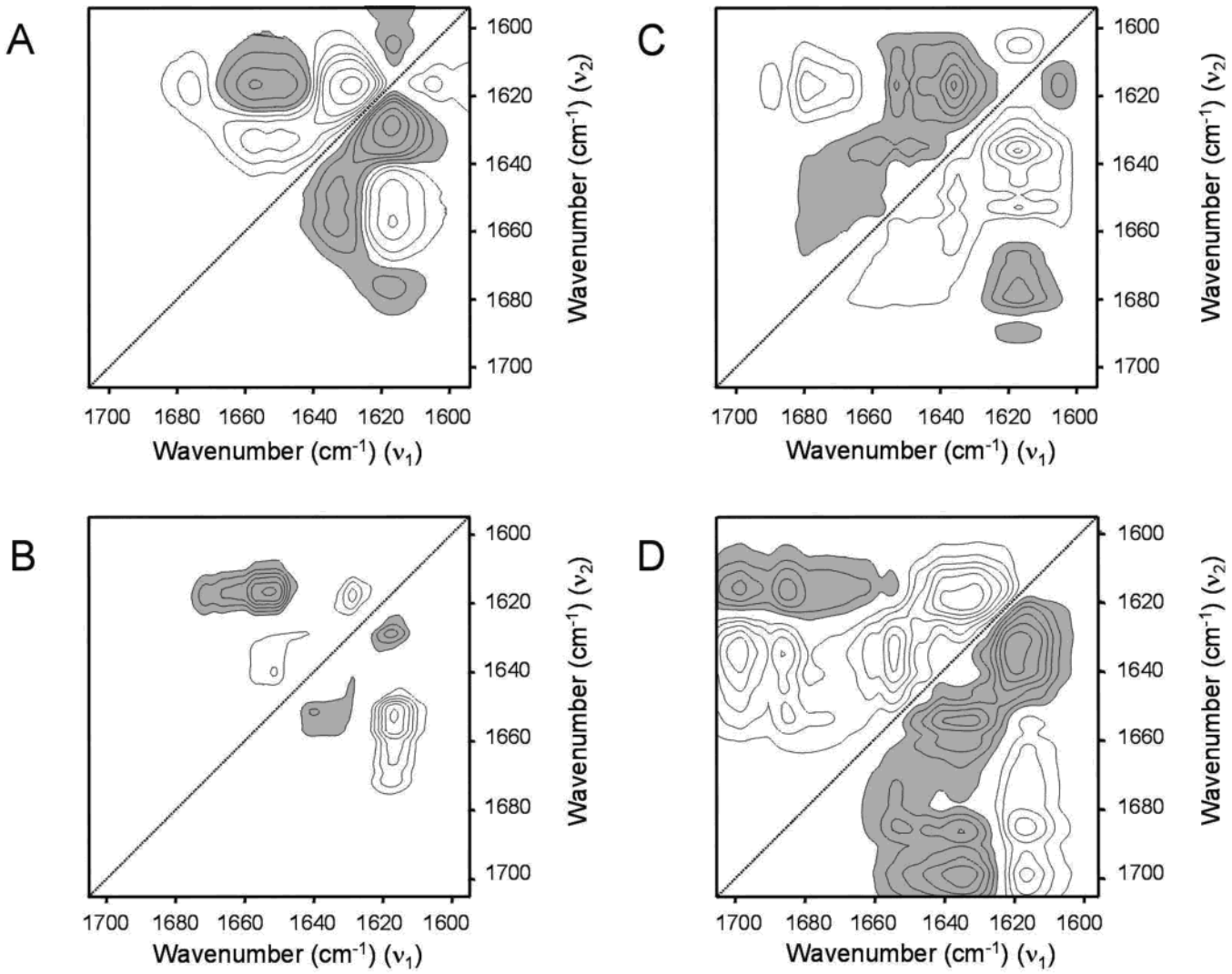

FIGURE 8: Asynchronous 2D-IR correlation spectra of the PKCα in D_2O buffer as a function of temperature variation between 20 and 75 °C in the presence of 200 μM EGTA (A), 600 μM Ca^{2+} (B), 500 μM PMA with 1 μM $ZnCl_2$ (C), and the combination of 250 μM Ca^{2+}, 500 μM ATP, 500 μM PMA, and 28.2 mM (20 mg·mL^{-1}) POPC/POPA (1:4 molar ratio) in the presence of 1 μM $ZnCl_2$ (D). The correlation spectra were obtained using the 2D-Pocha program. White and dark peaks are positive and negative correlations, respectively.

A point of controversy when performing quantitative studies of the secondary structure of proteins by curve fitting of the amide I band is whether the different components will have the same extinction coefficients (*45*, *56*, *57*) or not (*58*). Additional uncertainty comes from the fact that several works have been published reporting different values for these extinction coefficients (*58*−*60*). In this paper, we have used a method that assumes the simplest possibility, that is, that coefficients are not very different among them so that the error produced is not bigger than the intrinsic error of the method due to a number of other factors. It should be mentioned in support of this method that there is an increasing number of proteins that have been analyzed using it and the results obtained are in very good agreement with the structure reported for them using a high-resolution method like X-ray crystallography (*36*, *55*, *61*−*63*).

The Structure of PKCα in the Presence of EGTA. The high-resolution structure of PKCα is not yet known, so an estimation of its structure even at low resolution is useful. To this end, we have used a technique very well suited to calculate the secondary structures of proteins, Fourier transform infrared spectroscopy (FT-IR). The secondary structure thus described is the first estimation of the whole structure of a purified PKC. Although some previous studies on the secondary structure of PKC have been carried out using circular dichroism (*24*, *25*), these studies were performed using PKC purified from tissues that were mixtures of different isoenzymes. Therefore, the results obtained with the cloned and purified PKCα that we used are not fully comparable with previously published results. A summary of these results appear in Table 4, together with the results reported in this work and obtained through FT-IR.

We also include in Table 4 an estimation of the secondary structure of PKC obtained by means of an approximation using known high-resolution structures of PKC domains such as the pseudosubstrate (*64*), C1 (*11*, *65*), and C2 (*7*, *15*). The 3D structure of the catalytic domain is not known, and to estimate its structure, we used the information obtained from the catalytic domain of a related kinase, PKA (*19*), knowing the high sequence homology existing between both kinases (*18*). Adding all these fragments would give us a structure of 437 amino acid residues, meaning that a relatively large part (235 residues) remain unestimated, although most of this would presumably correspond to loops

Table 4: Comparison of PKCα Structures Obtained by Different Techniques

	secondary structure percentages				
	α-helix	β-sheet	β-turns	random coil and open loops	unknown
CD[a] (ref 24)	36	57	7	0	
CD (ref 25)[b]	40	*c*	*c*	*c*	
FT-IR (this study)[d]	22	49	7	22	
estimation adding known structures of domains	19	25	16	6	34

[a] Circular dichroism. [b] Without any addition. [c] Not determined. [d] In the presence of 200 μM EGTA at 20 °C.

and turns or random structures. According to these calculations, there are 124 residues in α-helix (12 from C1 domain, 9 from C2 domain, and 102 from the catalytic region), amounting to 19% of the total PKC structure. There are also 168 residues in β-sheet structure (39 from the C1 domain, 72 from the C2 domain, and 57 from the catalytic region) giving 25% of the total PKC. With respect to β-turns, there are 108 residues that adopt this secondary structure (35 from the C1 domain, 49 from the C2 domain, and 24 from the catalytic region), amounting to 16% of the total PKC structure. Finally, the pseudosubstrate region includes 37 residues in nonstructured configuration (6% of total PKC). If we look at Table 4, it is striking that the percentage of α-helix determined through circular dichroism is very high, especially when compared with those obtained by infrared spectroscopy and from the estimations made using the known domain structure. Note that the unknown structure (34%), obtained after the estimation from the high-resolution structures of the different PKC domains, is most likely to correspond to turns or random structures.

The 2D infrared correlation spectroscopy analysis yielded interesting information on the thermal unfolding process. The synchronous spectrum in the presence of EGTA that reflects the thermal denaturation of the protein, as the temperature increased from 20 to 75 °C, shows a negative correlation between α-helix and aggregated β-sheet, which means that one of these structures increases as the other one decreases during the thermal unfolding.

The asynchronous spectrum in the presence of EGTA during thermal denaturation shows that the unfolding follows a certain order with the aggregated β-sheet appearing after the changes in β-sheet. Other components, such as α-helix, changed before β-sheet.

The Structure of PKCα in the Presence of Ligands. We have seen that the presence of ligands affords some protection against the denaturation of PKCα, which is probably to be expected when monitoring binding to high-affinity sites in the protein, since most binding processes will not usually induce large changes in the secondary structure but are more likely to affect the 3D-folding. The binding of ligands may affect the coherence of the protein, in most cases increasing this character, and will hence protect it from thermal unfolding. It is interesting that Ca^{2+} efficiently protects the β-structure, whereas other ligands such as the combination of 250 μM Ca^{2+}, 500 μM ATP, 500 μM PMA, and 28.2 mM POPC/POPA in 1:4 molar ratio, in the presence of 1 μM $ZnCl_2$, offer a better protection to β-turns and α-helix structures, the last being most probably due to interaction with the phospholipids since the other ligands present in this mixture do not have this effect when assayed separately.

At difference with the study in the presence of EGTA, the synchronous spectrum in the presence of the combination of ligands in the same conditions shows that the aggregated β-sheet shows correlation not with α-helix but with β-sheet. This is in agreement with our FT-IR 1D analysis that suggests that the presence of the combination of ligands preserves the α-helix, probably due to the presence of phospholipids. According to the estimation of the secondary structure given in Table 4, most of the amino-acyl residues in α-helix belong to the catalytic domain, which, it has been proposed, binds to the membrane during PKC activation (*66*).

The asynchronous spectrum in the presence of Ca^{2+} was also different from that in the presence of EGTA, and the main correlation was between the aggregated β-sheet and the α-helix component, confirming our previous conclusion from the FT-IR 1D spectroscopic studies that Ca^{2+} somehow protects the β-sheet. It should be pointed out that Ca^{2+} is known to bind to the C2 domain, the structure of which is based on a β-sandwich (*7*), and we have already shown that Ca^{2+} protects this type of structure in the isolated C2 domain of PKCα from thermal denaturation (*62*, *63*). Therefore, it seems likely that the effect that we are observing in the whole enzyme is due to the C2 domain.

In summary, we have obtained interesting data with respect to the secondary structure of PKCα and its thermal unfolding, introducing a still new technique, 2D-IR spectroscopy, into the field and demonstrating its usefulness for dissecting complex interactions between proteins and ligands.

ACKNOWLEDGMENT

We thank Dr. Robert M. Bell (Duke University Medical Center, Durham, NC) for the kind gift of the porcine PKCα cDNA.

REFERENCES

1. Nishizuka, Y. (1995) *FASEB J. 9*, 484−496.
2. Mellor, H., and Parker, P. J. (1998) *Biochem. J. 332*, 281−292.
3. Newton, A. C. (2001) *Chem. Rev. 101*, 2353−2364.
4. Nishizuka, Y. (1992) *Science 258*, 607−614.
5. Parker, P. J., Coussens, L., Totty, N., Rhee, L., Young, S., Chen, E., Stabel, S., Waterfield, M. D., and Ullrich, A. (1986) *Science 233*, 853−859.
6. Coussens, L., Parker, P. J., Rhee, L., Yang-Feng, T. L., Chen, E., Waterfield, M. D., Francke, U., and Ullrich., A. (1986) *Science 233*, 859−866.
7. Verdaguer, N., Corbalán-García, S., Ochoa, W. F., Fita, I., and Gómez-Fernández, J. C. (1999) *EMBO J. 18*, 6329−6338.
8. Kikkawa, U., Takai, Y., Miyake, R., and Nishizuka, Y. (1983) *J. Biol. Chem. 258*, 11442−11445.
9. Taylor, S. S., and Radzio-Andzelm, E. (1994) *Structure 2*, 345−355.
10. Zhang, G., Kazaniet, M. G., Blumberg, P. M., and Hurley, J. H. (1995) *Cell 81*, 917−924.
11. Hommel, U., Zurini, M., and Luyten, M. (1994) *Struct. Biol. 1*, 383−387.
12. Xu, R. X., Pawelczyk, T., Xia, T., and Brown, S. C. (1997) *Biochemistry 36*, 10709−10717.
13. Sutton, R. B., and Sprang, S. R. (1998) *Structure 6*, 1395−1405.
14. Pappa, H., Murray-Rust, J., Dekker, L. V., Parker, P. J., and McDonald, N. Q. (1998) *Structure 6*, 885−894.
15. Ochoa, W. F., Corbalán-García, S., Eritja, R., Rodríguez-Alfaro, J. A., Gómez-Fernández, J. C., Fita, I., and Verdaguer, N. (2002) *J. Mol. Biol. 320*, 277−291.

16. Ochoa, W. F., García-García, J., Fita, I., Corbalán-García, S., Verdaguer, N., and Gómez-Fernández, J. C. (2001) *J. Mol. Biol. 311*, 837−849.
17. Corbalán-Garcia, S., García-García, J., Rodríguez-Alfaro, J. A., and Gómez-Fernández, J. C. (2003) *J. Biol. Chem. 278*, 4972−4980.
18. Orr, J. W., and Newton, A. C. (1994) *J. Biol. Chem. 269*, 27715−27718.
19. Knighton, D. R., Zheng, J., Ten Eyck, L. F., Ashford, V. A., Xuong, N.-H., Taylor, S. S., and Sowadski, J. M. (1991) *Science 253*, 407−414.
20. Srinivasan, N., Bax, B., Blundell, T. L., and Parker, P. J. (1996) *Proteins 26*, 217−235.
21. Newman, R. H., Carpenter, E., Freemont, P. S., Blundell, T. L., and Parker, P. J. (1994) *Biochem. J. 298*, 391−393.
22. Solodukhin, A. S., Caldwell, H. L., Sando, J. J., and Kretsinger, R. H. (2002) *Biophys. J. 82*, 2700−2708.
23. Owens, J. M., Kretsinger, R. H., Sando, J. J., and Chertihin, O. L. (1998) *J. Struct. Biol. 121*, 61−67.
24. Shah, J., and Shipley, G. G. (1992) *Biochim. Biophys. Acta 1119*, 19−26.
25. Boscá, L., and Morán, F. (1993) *Biochem. J. 290*, 827−832.
26. Arrondo, J. L. R., and Goñi, F. M. (1999) *Prog. Biophys. Mol. Biol. 72*, 367−405.
27. Noda, I. (1993) *Appl. Spectrosc. 47*, 1329−1336.
28. Noda, I., Dowerey, A. E., Marcott, C., Story, G. M., and Ozaki, Y. (2000) *Appl. Spectrosc. 54*, 236A−248A.
29. Ozaki, Y., Murayama, Wu, Y., and Czarnik-Matusewicz, B. (2003) *Spectrosc.: Int. J. 17*, 79−100.
30. Rebbechi, M., Peterson, A., and McLaughlin, S. (1992) *Biochemistry 31*, 12742−12747.
31. Sánchez-Piñera, P., Micol, V., Corbalán-García, S., and Gómez-Fernández, J. C. (1999) *Biochem. J. 337*, 387−395.
32. Micol, V., Sanchez-Piñera, P., Villalaín, J., de Godos, A., and Gómez-Fernández, J. C. (1999) *Biophys. J. 76*, 916−927.
33. Jiménez-Monreal, A. M., Aranda, F. J., Micol, V., Sánchez-Piñera, P., de Godos, A., and Gómez-Fernández, J. C. (1999) *Biochemistry 38*, 7747−7754.
34. Smith, P. K., Krohn, R. I., Hermanson, G. T., Mallia, A. K., Gartner, F. H., Provenzano, M. D., Fujimoto, E. K., Goeke, N. M., Olson, B. J., and Klenk, D. C. (1985) *Anal. Biochem. 150*, 76−85.
35. Conesa-Zamora, P., Gómez-Fernández, J. C., and Corbalán-García, S. (2000) *Biochim Biophys. Acta 1487*, 246−254.
36. Arrondo, J. L. R., Muga, A., Castresana, J., Bernabeu, C., and Goñi, F. M. (1989) *FEBS Lett. 252*, 118−120.
37. Powell, J. R., Wasacz, F. M., and Jakobsen, R. J. (1986) *Appl. Spectrosc. 40*, 359−444.
38. Griffiths, P. R., and Pariente, G. (1986) *Trends Anal. Chem. 5*, 209−215.
39. Arrondo, J. L. R., Castresana, J., Valpuesta, J. M., and Goñi, F. M. (1994) *Biochemistry 33*, 11650−11655.
40. García-García, J., Corbalán-García, S., and Gómez-Fernández, J. C. (1999) *Biochemistry 38*, 9667−9675.
41. Bandekar, J. (1992) *Biochim. Biophys. Acta 1120*, 123−143.
42. Bandekar, J., and Krimm, S. (1980) *Biopolymers 19*, 31−36.
43. Fabian, H., Naumann, D., Misselwitz, R., Ristau, O., Gerlach, D., and Welfle, H. (1992) *Biochemistry 31*, 6532−6538.
44. De las Rivas, J., and Barber, J. (1997) *Biochemistry 36*, 8897−8993.
45. Chehín, R., Iloro, I., Marcos, M. J., Villar, E., Shnyrov, V. L., and Arrondo, J. L. R. (1999) *Biochemistry 38*, 1525−1530.
46. Saba, R. I., Ruyschaert, J. M., Herschuelz, A., and Goormaghtigh, E. (1999) *J. Biol. Chem. 274*, 15510−15518.
47. Hadden, J. M., Bloemendal, M., Haris, P., Srai, S. K. S., and Chapman, D. (1994) *Biochim. Biophys. Acta 1205*, 59−67.
48. Krimm, S., and Bandekar, J. (1986) *Adv. Protein Chem. 38*, 181−364.
49. Muga, A., Arrondo, J. L. R., Bellon, T., Sancho, J., and Bernabeu, C. (1993) *Arch. Biochem. Biophys. 300*, 451−455.
50. Susi, H. (1972) *Methods Enzymol. 26*, 455−472.
51. Cladera, J., Galisteo, M. L., Sabes, M., Mateo, P. L., and Padros, E. (1992) *Eur. J. Biochem. 207*, 581−585.
52. Susi, H., Timasheff, S. N., and Stevens, L. (1967) *J. Biol. Chem. 242*, 5460−5466.
53. Surewicz, W. K., Leddy, J. J., and Mantsch, H. H. (1990) *Biochemistry 29*, 8106−8111.
54. Gorne-Tschelnokow, U., Naumann, D., Weise, C., and Hucho, F. (1993) *Eur. J. Biochem. 213*, 1235−1242.
55. Arrondo, J. L. R., Iloro, I., Aguirre, J., and Goñi, F. M. (2003) *Spectrosc.: Int. J.*, in press.
56. Arrondo, J. L. R., Muga, A., Castresana, J., and Goñi, F. M. (1993) *Prog. Biophys. Mol. Biol. 59*, 23−56.
57. Byler, D. M., and Susi, H. (1986) *Biopolymers 25*, 469−487.
58. De Jongh, H. H. J., Goormaghtigh, E., and Ruyschaert, J. M. (1996) *Anal. Biochem. 242*, 95−103.
59. Kabsch, W., and Sander, C. (1983) *Biopolymers 22*, 2577−2637.
60. Venyaminov, S. Y., and Kalnin, N. N. (1990) *Biopolymers 30*, 1259−1271.
61. Echabe, I., Haltia, T., Freire, E., Goñi, F. M., and Arrondo, J. L. R. (1995) *Biochemistry 34*, 13565−13569.
62. Corbalán-García, S., García-García, J., Sánchez-Carrillo, M., and Gómez-Fernández, J. C. (2003) *Spectrosc.: Int. J. 17*, 399−416.
63. Torrecillas, A., Corbalán-García, A., and Gómez-Fernández, J. C. (2003) *Biochemistry 42*, 11669−11681.
64. Nishikawa, K., Toker, A., Johannes, F. J., Songyang, Z., and Cantley, L. C. (1997) *J. Biol. Chem. 272*, 952−960.
65. Ichikawa, S., Hatanaka, H., Takeuchi, Y., Ohno, S., and Inagaki, F. (1995) *J. Biochem. (Tokyo) 117*, 566−574.
66. Zidovetzki, R., and Lester, D. S. (1992) *Biochim. Biophys. Acta 1134*, 261−272.

BI035128I